SCIENCE CHINA
Information Sciences

• LETTER •

June 2026, Vol. 69, Iss. 6, 169402:1–169402:2
https://doi.org/10.1007/s11432-025-4769-2

Wide-range 3D printed stretchable triboelectric sensor for multi-parameter body monitoring and intelligent human-machine interaction

Yun YANG[1*], Ziheng WANG[1], Tingting CAI[2*], Shuping XUE[1], Zhibang ZHANG[1], Zongwei ZHANG[3], Yingying ZHANG[1] & Hui LI[1]

[1]*Department of Resource and Mechanical Engineering, Lyuliang University, Lvliang 033001, China*
[2]*Department of Chemical and Material Engineering, Lyuliang University, Lvliang 033001, China*
[3]*Ji Hua Laboratory, Foshan 528200, China*

Received 26 September 2025/Revised 7 December 2025/Accepted 19 January 2026/Published online 8 May 2026

Citation Yang Y, Wang Z H, Cai T T, et al. Wide-range 3D printed stretchable triboelectric sensor for multi-parameter body monitoring and intelligent human-machine interaction. Sci China Inf Sci, 2026, 69(6): 169402, https://doi.org/10.1007/s11432-025-4769-2

With the rapid evolution of the Internet of Things (IoT) and artificial intelligence (AI), the demand for wearable electronics facilitating comprehensive health monitoring and intuitive human-machine interaction (HMI) has surged [1]. Triboelectric nanogenerators (TENGs) hold significant promise as a viable technology for self-powered sensing within this paradigm [2, 3]. Nevertheless, reconciling cost-effectiveness, stretchability, sensitivity, and a broad detection range remains a formidable challenge for 3D-printed flexible TENGs [4]. Existing devices are often constrained by the intrinsic rigidity of commercial filaments or the structural incongruity of multi-material interfaces [5], impeding the simultaneous resolution of micro-physiological signals (e.g., pulse, ∼0.01 N) and vigorous body movements (>100 N). To transcend this limitation, we present a low-cost, 3D-printed stretchable triboelectric sensor (3DPS-sensor) featuring an ultra-wide linear sensing range (0.01–300 N), thereby enabling diverse applications ranging from precision traditional Chinese medicine (TCM) pulse diagnostics to high-load robotic control.

Fabrication and design. The 3DPS-sensor is manufactured via a commercial fused deposition modeling (FDM) 3D printer (Figure 1(a)). A thermoplastic polyurethane (TPU) filament, doped with a conductive carbon black network, constructs the electrode. To mitigate the limited stretchability inherent to standard FDM parts, we engineered an optimized S-shaped electrode geometry. Comparative mechanical analysis (Figure A1) confirms that this S-shaped design exhibits superior mechanical compliance under stretching relative to zigzag or square-wave patterns. The electrode, featuring six semi-circular bends, is fully encapsulated within a silicone rubber matrix (Ecoflex 00-30), which functions dualistically as the negative triboelectric layer and protective packaging. Material characterization (Figure A2) corroborates the composition: Py-GC/MS analysis identified characteristic tetrahydrofuran peaks, confirming the polyether-based nature of the TPU, while SEM-EDS mapping revealed a homogeneous distribution of carbon (76.06 wt%) within the matrix, ensuring a robust percolation network for charge transfer. The device affords versatile form factors, including a "film form" for patch applications and a "sleeve form" for digital/wrist wear. The sensor demonstrates exceptional mechanical resilience, sustaining up to 100% tensile strain, 720° torsion, and arbitrary bending without electrical failure. Comprehensive characterization data are provided in Appendix A.

Sensing performance. Operating in single-electrode mode, the 3DPS-sensor exhibits a robust electrical response. A defining feature of this device is its distinctively wide sensing range. As depicted in Figure 1(b) and Figure B1(a), the open-circuit voltage follows a piecewise linear relationship with applied force (5–300 N). In the low-force regime (<110 N), sensitivity reaches 0.459 V/N, attributed to the rapid expansion of the effective contact area between the micro-rough surfaces of the silicone and skin. In the high-force regime (110–300 N), sensitivity stabilizes at 0.045 V/N as material deformation approaches saturation. Crucially, the detection limit extends down to ∼0.01 N, a capability validated by the distinct signal generated from a 0.0097 g micro-particle impact. Applying the impulse-momentum theorem ($F\Delta t = \Delta p$) with the measured impact duration ($\Delta t \approx 0.08$ s, Figure 1(b) bottom), the estimated dynamic force is below 0.01 N, confirming the sensor's micro-force detection capability (Figure B2). As detailed in Table B1, unlike most FDM sensors restricted to narrow sensing ranges (<50 N), the 3DPS-sensor achieves an ultra-wide range (0.01–300 N). Furthermore, it exhibits a highly linear response to tensile strain (20%–100%) with a high coefficient of determination ($R^2 > 0.98$, Figure B1(b)). Simultaneously, the output voltage shows negligible dependence on excitation frequency (1–3 Hz, Figure B1(c)). Durability tests confirmed consistent output after 10000 compression cycles and 1000 stretching cycles (Figure B3). Detailed performance data are available in Appendix B.

Physiological monitoring and TCM application. Leveraging its high sensitivity to micro-forces, the 3DPS-sensor was deployed for digitized TCM pulse diagnostics. We designed a custom sensor array to monitor three distinct radial artery sites: "Cun", "Guan", and "Chi". The system captured high-fidelity pulse waveforms containing rich hemodynamic features, enabling the algorithmic

* Corresponding author (email: yangyun@llu.edu.cn, Caitt1422@foxmail.com)

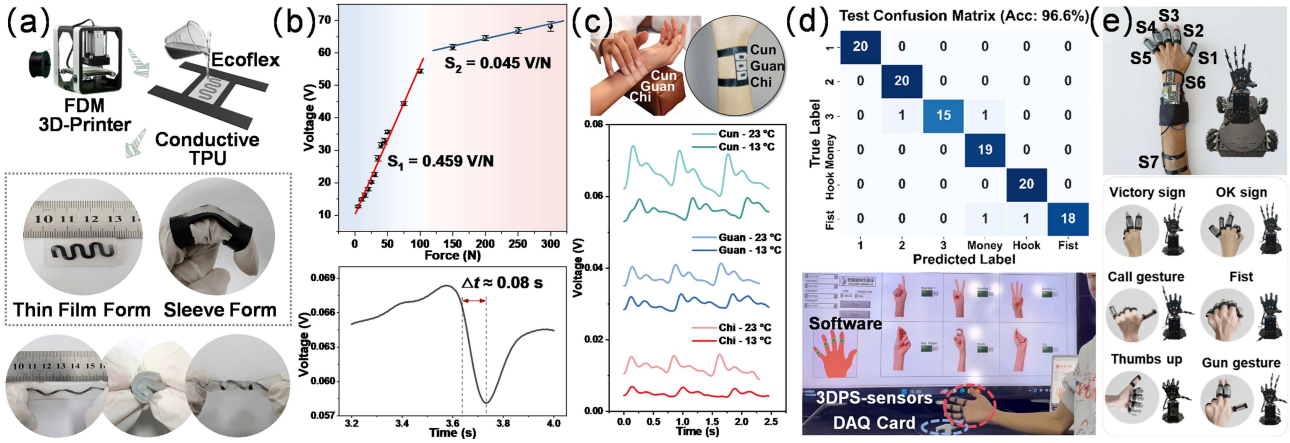

Figure 1 (Color online) Fabrication, wide-range sensing performance, and multi-scenario applications of the 3DPS-sensor. (a) Schematic of the FDM printing process (top) and optical images of the sensor in thin-film and sleeve forms demonstrating high flexibility (bottom); (b) wide-range linearity (0–300 N) showing two sensitivity regions (top) and the voltage response to a micro-force impact with ∼0.08 s response time (bottom); (c) TCM pulse diagnosis application: sensor placement at "Cun", "Guan", and "Chi" loci (top) and pulse waveforms recorded under different ambient temperatures (bottom); (d) test confusion matrix of the gesture recognition system achieving 96.6% accuracy and the corresponding real-time software interface; (e) HMI demonstration: wearable system layout and bionic hand control using distinct gestures.

separation of respiratory and pulse signals (Figure C1). The system successfully distinguished hemodynamic variations induced by cold stimulation. As shown in Figure 1(c) (bottom) and Figure C2, when the ambient temperature dropped from 23°C to 13°C, the wave amplitudes at all three sites decreased significantly. This observation corroborates the physiological mechanism of cold-induced vasoconstriction and the TCM theory of "cold coagulation". Quantitative analysis confirmed that the fundamental frequencies of heart rate and respiration rate collected by the sensor closely matched those of a commercial medical monitor, with high Pearson correlation coefficients ($r > 0.97$, Figure C3), validating its potential for objective, digitized TCM diagnosis. Beyond micro-signals, the sensor's utility extends to macro-scale motion monitoring. As illustrated in gait analysis (Figure C4), the sensor attached to a shoe heel distinctively recognized five motion states, with peak voltages surging from ∼20 V during walking to over 100 V during jumping. Furthermore, Figure C5 demonstrates real-time monitoring of elbow and knee joints, where the output voltage correlates positively with the bending angle. Supporting data are detailed in Appendix C.

Gesture recognition application. To exemplify precision in capturing kinematic features, we developed a smart glove integrated with four 3DPS-sensors (Figure D1(a)) to monitor finger bending and intelligently recognize six gestures. We established an 11-dimensional feature vector for each gesture, comprising parameters such as peak amplitude, motion frequency, and inter-finger time lag (Figure D1(b)). These features were processed via a support vector machine (SVM) classifier utilizing a radial basis function (RBF) kernel. The model achieved a 96.6% recognition accuracy across six distinct categories (Figure 1(d)). To ensure robustness against environmental humidity variations, we implemented an L2-norm normalization strategy for feature processing. Notably, as illustrated in Figure D2, increasing relative humidity from 10% to 50% caused a significant attenuation in raw voltage due to surface charge leakage. However, the normalization strategy effectively mitigated this drift, thereby creating a humidity-invariant feature space that preserves recognition stability under fluctuating environmental conditions (Figures D1(c), (d) and Table D1). Detailed algorithmic explanations are provided in Appendix D.

Human-machine interaction application. Building upon this recognition capability, we designed a fully integrated wearable teleoperation system. The sensor array was expanded to seven units (S1–S7) to envelop the fingers, wrist, and elbow. The data processing unit was miniaturized using an ESP32 microcontroller, implementing a dual-stage filtering logic: a 0.5 s moving average window followed by a voltage threshold strategy. Mapped commands were transmitted wirelessly via Bluetooth to a mobile robotic platform. As shown in Figure 1(e) and Figure E1, users successfully navigated the robot and manipulated a robotic arm using intuitive gestures. Further details are provided in Appendix E.

Conclusion. In summary, we have developed a commercially viable 3D-printed stretchable triboelectric sensor that bridges the gap between micro-force physiological sensing and high-load motion monitoring. By integrating a novel S-shaped conductive TPU electrode with a silicone rubber matrix, the monolithic device achieves exceptional mechanical compliance (100% tensile strain, 720° torsion) and robust durability (10000 cycles). With a high sensitivity of 0.459 V/N and a low detection limit of 0.01 N, it enables diverse applications ranging from digitized TCM pulse diagnostics consistent with commercial devices to AI-enhanced gesture recognition and HMI systems with 96.6% accuracy. This work provides a scalable, low-cost manufacturing route for next-generation multi-functional wearable electronics.

Acknowledgements This work was supported by Fundamental Research Program of Shanxi Province (Grant Nos. 202303021212285, 202303021212284) and Key R&D Project of Lvliang City (Grant Nos. 2024RC25, 2023RC17).

Supporting information Appendixes A–E and Videos 2, 4. The supporting information is available online at info.scichina.com and link.springer.com. The supporting materials are published as submitted, without typesetting or editing. The responsibility for scientific accuracy and content remains entirely with the authors.

References

1 Xu C, Solomon S A, Gao W. Artificial intelligence-powered electronic skin. Nat Mach Intell, 2023, 5: 1344–1355
2 Li Y, Gu Y Z, Qian S, et al. A stretchable, ionic conductive, and adhesive patch electrode with ultra-low on-skin impedance for electrophysiological signal recording. Sci China Inf Sci, 2025, 68: 129402
3 Pu X, Zhang C, Wang Z L. Triboelectric nanogenerators as wearable power sources and self-powered sensors. Natl Sci Rev, 2023, 10: nwac170
4 Mahmud M A P, Zolfagharian A, Gharaie S, et al. 3D-printed triboelectric nanogenerators: state of the art, applications, and challenges. Adv Energy Sustain Res, 2021, 2: 2000045
5 Wang S, Zeng R, Ding X, et al. Flexible triboelectric sensor array based on 3D printed bead-on-string sacrificial layer for human-machine interactions. Nano Energy, 2024, 122: 109318